Numerical Simulations of HC-PCF Filled with Different Liquids for Sensing Applications

Zeina Khalifa[1*], Hussein T. Saloom[2**], Saif A. Mohammed[3], Ahmad K. Ahmad[1]

[1]Department of Physics, College of Science, Al Nahrain University, Jadriah P. O. Box 64055, Baghdad, Iraq
[2]Al-Nahrain Nanorenewable Research Center, Al-Nahrain University, Baghdad, Iraq
[3]University of Baghdad, Institute of Laser for Postgraduate Studies, Baghdad, Iraq
Email address: *zeina767@yahoo.com, **hussein_thamer@yahoo.com

Abstract— A numerical analysis using finite element method (FEM) are used to simulate hollow core photonic crystal fiber (HC-PCF) overfilled with various liquids (heavy water, water and pentanol). Two type of the HC-PCF are used the HC19-1550 and HC-1550. The effective mode index and the confinement loss of the fundamental mode for empty fiber and infiltrated PCF are numerically calculated. The results show that the effective mode index increases with increase of refractive index and the minimal value of confinement loss are not only decreases but also shifted to smaller wavelengths which allow as to determine the amplitude sensitivity of the fiber.

Keywords— Hollow core photonic crystal fiber;finite element method sensitivity;confinement loss.

I. INTRODUCTION

Photonic crystal fiber (PCF) is a new class of optical fiber which is one of the recent inventions in the field of fiber optics. PCF can be used as a transmission media as well as optical functional devices. In contrast to the conventional optical fiber, PCFs have additional design features, such as air-hole diameter, pitch size, and number of rings, which offer to overcome many limitations of conventional fiber. PCF can be divided into two main class, Hollow core fibers and solid core fibers. In solid core fiber, the refractive index of the core is higher than the refractive index of cladding so the light can be guided by total internal refraction. Hollow core PCF provide light confinement in a low refractive index core exploiting the photonic band gap mechanism, which is due to the presence of a periodic lattice of holes in the cladding [1]. PCF based sensors are smart applications in fiber optic technology which have been investigating and developing since last decade. A wide range of sensing applications of PCF are available, such as temperature sensors, refractive index (R.I) sensors [2], chemical sensors [3], mechanical sensors [4], pressure sensors [5], gas sensors [6, 7], stress sensors [8], pH sensors [9], liquid sensors [10], biosensors [11]. Photonic crystal fiber based liquid and gas sensors through the evanescent field show excellent performance in terms of sensitivity, because core of the PCF directly interacts with the material to be analysed.

II. FINITE ELEMENT METHOD

Finite element method is a powerful tool to cope with any kind of geometry and to provide a full vector analysis [12]. The properties of propagating mode of the proposed PCFs sensor are numerically investigated. We have considered circular perfectly matched layer (PML) as a boundary condition. The cross sections of the proposed PCFs are divided into homogeneous triangular subspaces. The liquid filled air holes' region is then divided into many sub-domains which are either triangular or quadrilateral in shape. Using FEM, Maxwell's equations are solved by accounting neighbouring subspaces. The modal analysis has been performed in the x-y plane of the PCF structure. The following vectorial wave equation can be derived from the Maxwell's equation [13].

$$\nabla \times (S^{-1} \nabla \times E) - k^2_0 \, n^2 \, SE = 0 \tag{1}$$

where S represents the PML matrix of 3×3 and S^{-1} is the inverse of S matrix. The symbol E denotes the electric field vector, n is the refractive index of the domain, k_0 is the wave number in free space, and λ is the operating wavelength. The propagating constant β is represented by the following equation.

$$\beta = n_{eff} \, k_0 \tag{2}$$

Due to the finite number of air holes in the cladding part, there may cause leakage of light. The leakage of light from core to exterior materials results in confinement loss (dB/m) which can be obtained from the imaginary part of n_{eff} by using the following equation [14].

$$CL = 8.686 \times k_0 \, . \, I_m(n_{eff}) \tag{3}$$

However, this leakage of light energy can be omitted by using an infinite number of air holes. But in practical, the number of air holes is finite.

In the present work, specific two kinds of hollow core PCF considered, that is HC19-1550 figure 1(a), having a diameter of the holey region of 72.38 μm, core diameter of 20.806 μm and air holes spacing of 4.053 μm and HC-1550 figure 1(b), having a diameter of the holey region of 71.47μm, core diameter of 12 μm and air holes spacing of 4.194 μm.
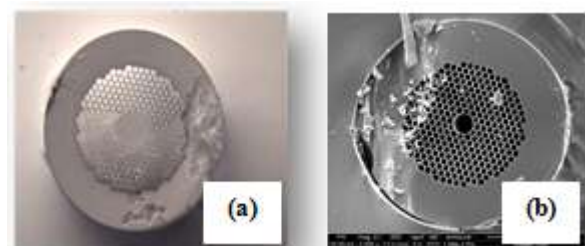
Fig. 1. (a) HC19-1550 (b) HC-1550 under microscope.

The refractive index of silica and of the three filling liquids, (heavy water, water and pentanol) as function of

253

Zeina Khalifa, Hussein T. Saloom, Saif A. Mohammed, and Ahmad K. Ahmad, "Numerical simulations of HC-PCF filled with different liquids for sensing applications," *International Research Journal of Advanced Engineering and Science*, Volume 3, Issue 1, pp. 253-257, 2018.

wavelengths between 600 to 1600 nm are plotted as presented in figure (2) [15-18]. One can recognize from this figure that the refractive index decreases with increasing the wavelength, and the refractive index of the used liquids are less than that of silica.
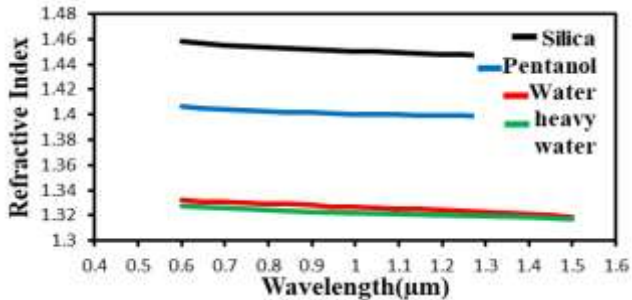
Fig. 2. Refractive index of silica, pentanol, water heavy and water.

III. SIMULATION RESULTS

HC19-1550: The simulation steps of optical behavior of PCF are present in figure (3). A simple example of a HC19-1550 PCF when empty, was made from silica having a hexagonal array of air holes a long it's length with central 20 μm hollow core. The Cladding geometry of PCF with refractive index of air =1.00027326 are shown in figure (3b). The structure of designed hollow core PCF with refractive index of silica glass to core and cladding n=1.4440 is presented in figure (3c). The structure of hollow core PCF immersed in the external solution with refractive index 1.38is presented in figure (3d). The finite element mesh of PCF are presented in figure (3e).
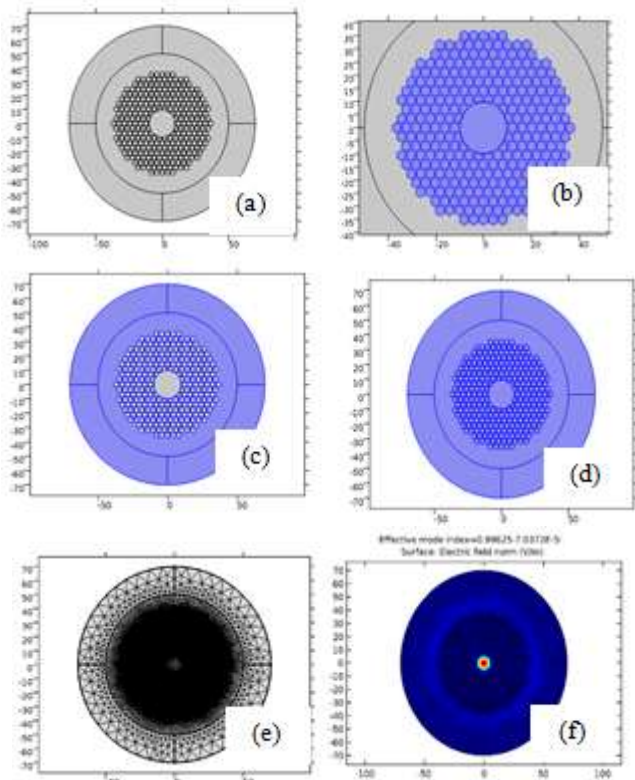
Fig. 3. (a) The structure of designed HC19-1550 PCF (b) The geometry of cladding PCF with nair =1.00027326 (c) The structure of designed HC-PCF

with refractive index of silica glass to core and cladding n=1.4440 (d) The structure of HC-PCF immersed in the external solution with refractive index 1.38 (e) FEM-Mesh of PCF (f) The fundamental mode when the PCF empty.

From figure (3.f) it's clear that there is effective mode index which contain real and imaginary part, the complex effective refractive index of the proposed sensor which is a function of both the material and waveguide contributions. The variations of real parts of effective indices with wavelength for HC19-1550 PCF infiltrated with heavy water, water and pentanol are presented in figure (4). It's clear that effective index n_{eff} decreased as wavelength increased.
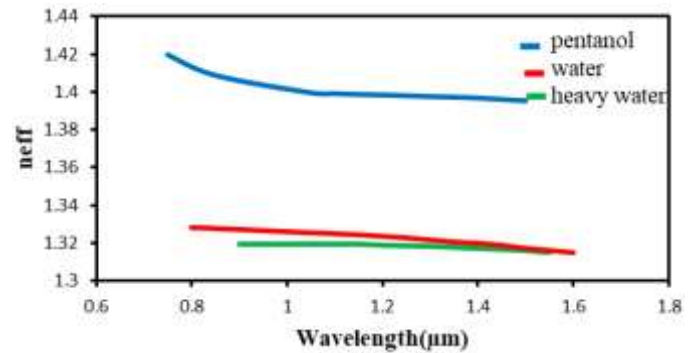
Fig. 4. Effective refractive index of pentanol, water and heavy water.

From the imaginary part of the effective mode index, confinement loss (CL) is calculated based on eq. (3). The confinement losses of the fundamental modes for the proposed infiltrated HC19-1550 PCF with different liquids are presented in figure (5).
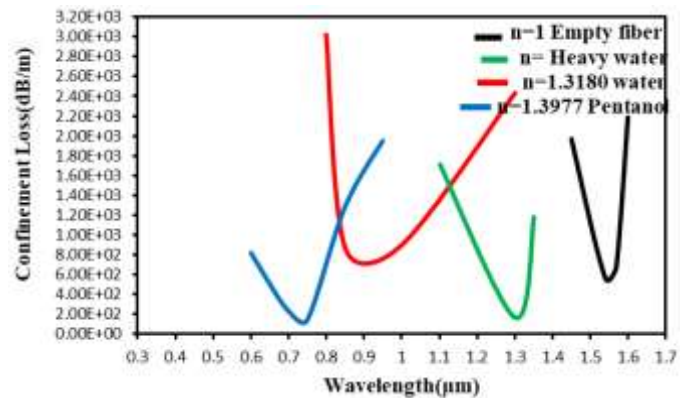
Fig. 5. confinement loss of the fundamental mode for different refractive indices (different liquids) infiltrated HC19-1550 PCF.

Values decreasing as refractive index of air holes' increases. By changing the refractive index of the cladding, the photonic band gap peak position is manipulated which results in a possibility to choose the suitable wavelength with minimum confinement loss.

The performance of the PCF can be measured by the sensitivity. We analysed the sensitivity of the proposed fiber by using wavelength interrogation and amplitude interrogation. In wavelength interrogation, wavelength sensitivity can be computed by the following formula [19]:

$$S_\lambda \left(\frac{nm}{RIU}\right) = \Delta\lambda_{peak}/\Delta n_a \qquad (4)$$

where $\Delta\lambda_{peak}$ is the difference between peak wavelength shifts and Δn_a is the variation of analyte RI. The change in the analyte RI are 1.3170- 1.3180 and 1.3180-1.3977 which equal (0.001and ,0.0797). So the calculated wavelength sensitives are 400.054 and 1882.05. The resolution of the sensor is another important parameter that represents how a small change of analyte RI can be detected by the sensor. The resolution of the proposed sensor can be obtained by the given the following formula [20]:

$$R(RIU) = \Delta n_a \, x \, \Delta\lambda_{min}/\Delta\lambda_{peak}. \qquad (5)$$

Assuming that Δn_a is the variation of analyte RI for different liquids, $\Delta\lambda_{min}= 0.1$ [21] (This is a standard assumption value for the minimum spectral resolution) and $\Delta\lambda_{peak}$ is the difference between peak wavelength shifts. We found the resolution of the proposed of the proposed sensors are $2.5x10^{-7}$ and $5.31x10^{-5}$. Amplitude interrogation can solve this issue by measuring sensitivity at a specific wavelength. The amplitude sensitivity can be obtained by the following equation [21].

$$S_A(RIU^{-1}) = -\frac{1}{\alpha(\lambda, n_a)} \frac{\partial\alpha(\lambda, n_a)}{\partial n_a} \qquad (6)$$

where $\alpha(\lambda, n_a)$ is the overall propagation loss at RI of n_a and $\partial\alpha(\lambda, n_a)$ is the loss difference between two loss spectra. It can be observed from Figure (6a) that loss depth can be increased by increasing the analyte RI. Increasing the value of n_a leads to a reduction of the index contrast between the core and cladding, which leads to an increase in confinement loss. The lowest confinement loss of $1.46*10^2$ dB/m was found for an analyte RI of 1.3977 at 0.75 µm.
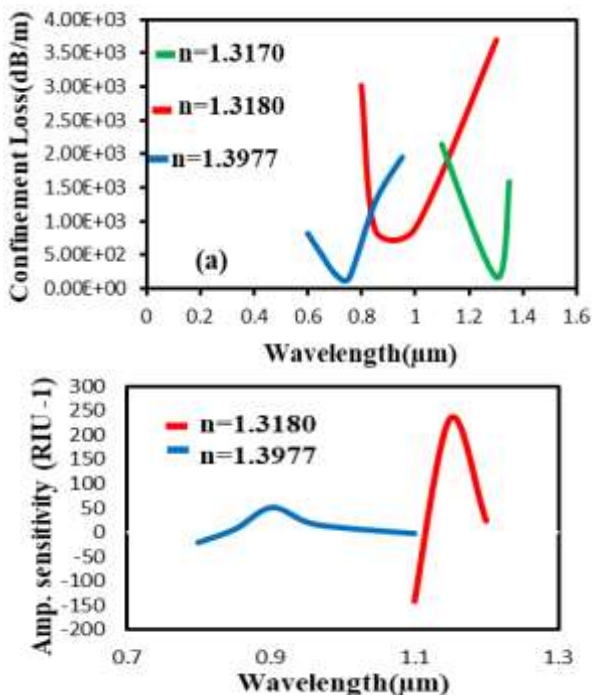
Fig. 6. (a) Fundamental loss variation for increasing analyte RI from 1.3170 to 1.3977 and (b) Amplitude sensitivity for different analyte RI.

Figure (6) b depicts the amplitude sensitivity of the proposed sensor for different analyte RI values. We found a maximum amplitude sensitivity of about 235.29 RIU^{-1} at 1.15 µm for an analyte RI of 1.3180. Now if we compare the results of the fundamentals mode for the three different liquids with their electric field, we will find the water has a best electric field than other liquids as presented in figure (7).

Heavy Water   **Water**
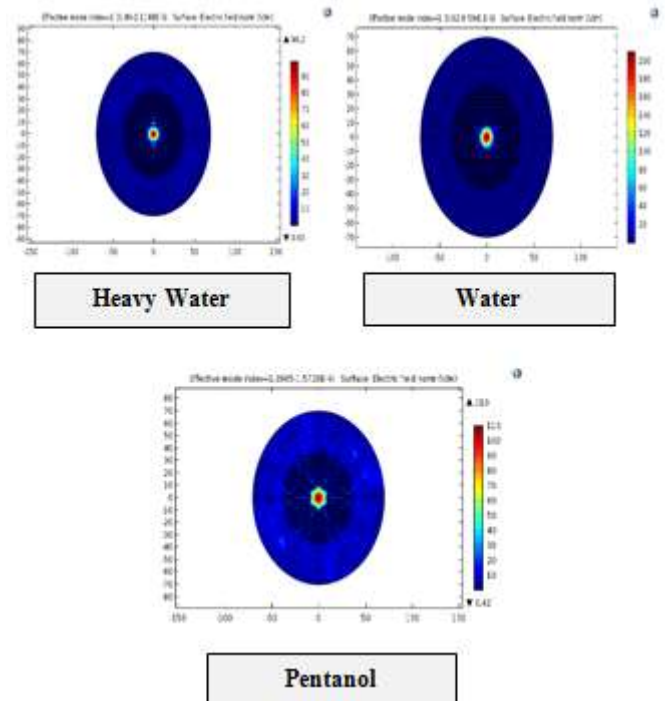
Pentanol

Fig. 7. Fundamentals mode for different liquids of HC19-1550(heavy water, water and pentanol).

From figure (7) we found the water has a best electric field than other liquids equal to 200 V/m which lead to high sensitivity.

HC-1550:

The fundamental mode of HC-1550 PCF when the PCF empty is presented in figure (8).
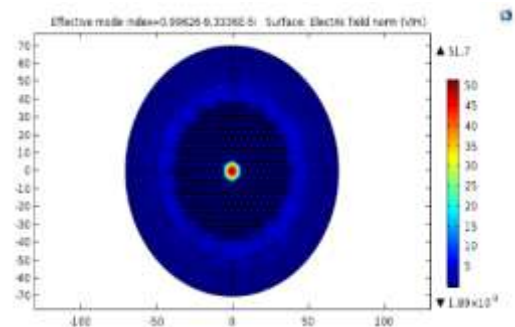
Fig. 8. Fundamental mode of the HC-1550 PCF when the PCF is empty.

From the imaginary part of the effective mode index, confinement loss (CL) is calculated based on eq. (3). The confinement loss of the fundamental mode for the proposed HC-1550 PCF is presented in figure (9).

255

Zeina Khalifa, Hussein T. Saloom, Saif A. Mohammed, and Ahmad K. Ahmad, "Numerical simulations of HC-PCF filled with different liquids for sensing applications," *International Research Journal of Advanced Engineering and Science*, Volume 3, Issue 1, pp. 253-257, 2018.
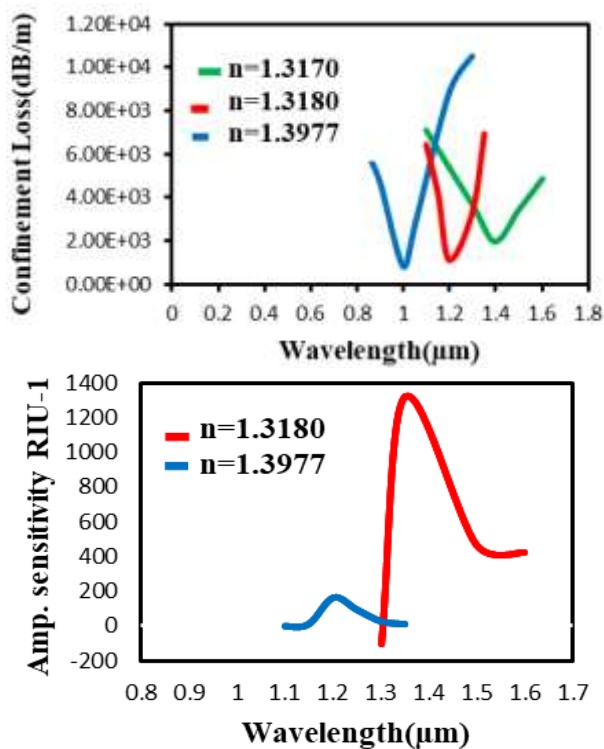
Fig. 9. (a) Fundamental loss variation for increasing analyte RI from 1.3170 to 1.3977 and (b) amplitude sensitivity for different analyte RI.

From figure (9.a) by applying eq. (4) the wavelength sensitives are 200000 and 2509.41 nm/ RIU. From eq. (6) the maximum amplitude sensitivity is 1320 RIU^{-1} at 1.35 μm for an analyte RI of 1.3180 for water. Also the resolution of the proposed sensor is $5x10^{-7}$ and $3.99x10^{-5}$. Figure (10) shows the comparison of the fundamental mode of liquids with their electric field.
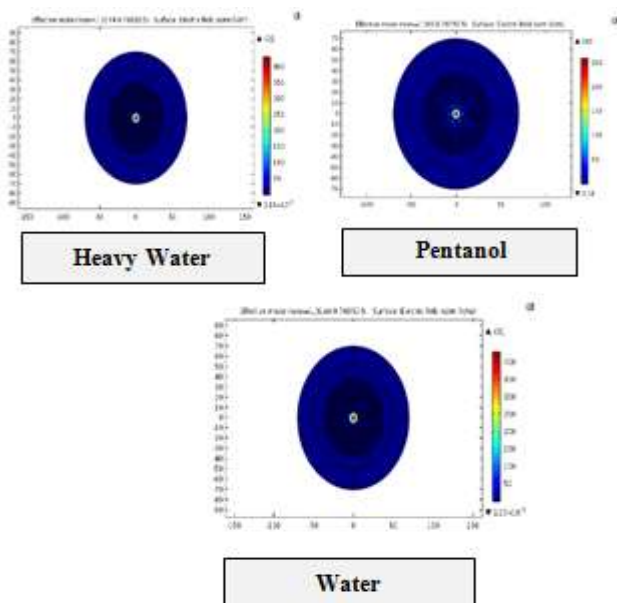
Fig. 10. Fundamentals mode for different liquids of HC-1550(heavy water, water and pentanol).

We found that the water has a best electric field than other liquids equal to 431 V/m which leads to high sensitivity, that's mean whenever the liquid has best electric field it will has a higher sensitivity than other liquids.

IV. CONCLUSION

The confinement loss of the fundamental mode for hollow core PCF was numerically analyzed using the FEM. By testing different refractive indices (heavy water, water and pentanol), the effective mode index increases with the increase of refractive index in the holey region. The position of transmission window with minimum confinement loss was shifted to lower wavelengths and this has facilitated the calculation of the sensitivity. In HC19-1550 fiber the maximum amplitude sensitivity is 235.29 RIU^{-1} at 1.15 μm for an analyte RI of 1.3180 (for water) with resolution of $2.5x10^{-7}$ and the electric field value is 200 V/m. In HC-1550 fiber the maximum amplitude sensitivity is 1320 RIU^{-1} at 1.35 μm for an analyte RI of 1.3180 (for water) with resolution of $5x10^{-7}$ and the value of the electric field is 431 V/m which is a better results than HC19-1550.

REFRENCES

[1] Smolka, S., Barth, M., & Benson, O. (2007). Highly efficient fluorescence sensing with hollow core photonic crystal fibers. Optics Express, 15(20), 12783-12791.
[2] Liu, Y., & Salemink, H. W. M. (2014). All-optical on-chip sensor for high refractive index sensing in photonic crystals. EPL (Europhysics Letters), 107(3), 34008.
[3] Zheng, S., Zhu, Y., & Krishnaswamy, S. (2012, March). Nanofilm-coated photonic crystal fiber long-period gratings with modal transition for high chemical sensitivity and selectivity. In Smart Sensor Phenomena, Technology, Networks, and Systems Integration 2012 (Vol. 8346, p. 83460D). International Society for Optics and Photonics.
[4] Xi, X., Wong, G. K., Weiss, T., & Russell, P. S. J. (2013). Measuring mechanical strain and twist using helical photonic crystal fiber. Optics letters, 38(24), 5401-5404.
[5] Lee, C., & Thillaigovindan, J. (2009). Optical nanomechanical sensor using a silicon photonic crystal cantilever embedded with a nanocavity resonator. Applied optics, 48(10), 1797-1803.
[6] Olyaee, S., & Dehghani, A. A. (2013). Ultrasensitive pressure sensor based on point defect resonant cavity in photonic crystal. Sensor Letters, 11(10), 1854-1859.
[7] Zhang, Y. N., Zhao, Y., & Wang, Q. (2013). Multi-component gas sensing based on slotted photonic crystal waveguide with liquid infiltration. Sensors and Actuators B: Chemical, 184, 179-188.
[8] Morshed, M., Arif, M. F. H., Asaduzzaman, S., & Ahmed, K. (2015). Design and characterization of photonic crystal fiber for sensing applications. European Scientific Journal, ESJ, 11(12).
[9] Lu, T. W., & Lee, P. T. (2009). Ultra-high sensitivity optical stress sensor based on double-layered photonic crystal microcavity. Optics express, 17(3), 1518-1526.
[10] Hu, P., Dong, X., Wong, W. C., Chen, L. H., Ni, K., & Chan, C. C. (2015). Photonic crystal fiber interferometric pH sensor based on polyvinyl alcohol/polyacrylic acid hydrogel coating. Applied optics, 54(10), 2647-2652.
[11] Akowuah, E. K., Gorman, T., Ademgil, H., Haxha, S., Robinson, G. K., & Oliver, J. V. (2012). Numerical analysis of a photonic crystal fiber for biosensing applications. IEEE Journal of Quantum Electronics, 48(11), 1403-1410.
[12] Koshiba, M., & Inoue, K. (1992). Simple and efficient finite-element analysis of microwave and optical waveguides. IEEE Transactions on Microwave Theory and Techniques, 40(2), 371-377.
[13] Cucinotta, A., Selleri, S., Vincetti, L., & Zoboli, M. (2002). Holey fiber analysis through the finite-element method. IEEE Photonics Technology Letters, 14(11), 1530-1532.

256

[14] Ademgil, H. (2014). Highly sensitive octagonal photonic crystal fiber based sensor. Optik-International Journal for Light and Electron Optics, 125(20), 6274-6278.

[15] Kedenburg, S., Vieweg, M., Gissibl, T., & Giessen, H. (2012). Linear refractive index and absorption measurements of nonlinear optical liquids in the visible and near-infrared spectral region. Optical Materials Express, 2(11), 1588-1611.

[16] Moutzouris, K., Papamichael, M., Betsis, S. C., Stavrakas, I., Hloupis, G., & Triantis, D. (2014). Refractive, dispersive and thermo-optic properties of twelve organic solvents in the visible and near-infrared. Applied Physics B, 116(3), 617-622.

[17] Hale, G. M., & Querry, M. R. (1973). Optical constants of water in the 200-nm to 200-μm wavelength region. Applied optics, 12(3), 555-563.

[18] Kedenburg, S., Vieweg, M., Gissibl, T., & Giessen, H. (2012). Linear refractive index and absorption measurements of nonlinear optical liquids in the visible and near-infrared spectral region. Optical Materials Express, 2(11), 1588-1611.

[19] Rifat, A.A.; Mahdiraji, G.A.; Chow, D.M.; Shee, Y.G.; Ahmed, R.; Adikan, F.R.M. "Photonic Crystal Fiber-Based Surface Plasmon Resonance Sensor with Selective Analyte Channels and Graphene-Silver Deposited Core", Sensors, **15**, (2015) 11499–11510.

[20] Wang, G., Li, S., An, G., Wang, X., Zhao, Y., Zhang, W., & Chen, H. (2016). Highly sensitive D-shaped photonic crystal fiber biological sensors based on surface plasmon resonance. Optical and Quantum Electronics, 48(1), 46.

[21] Rifat, A.A.; Mahdiraji, G.A.; Ahmed, R.; Chow, M.D.; Sua, Y.M.; Shee, Y.G. "Copper-graphene based photonic crystal fiber plasmonic biosensor", IEEE Photonics J., 8, (2016) 4800408.